Article

Influence of Abrasive Waterjet Parameters on the Cutting and Drilling of CFRP/UNS A97075 and UNS A97075/CFRP stacks.

Raul Ruiz-Garcia [1], Pedro F. Mayuet [1,*], Juan Manuel Vazquez-Martinez [1] and Jorge Salguero Gómez [1]

[1] Department of Mechanical Engineering & Industrial Design, Faculty of Engineering, University of Cadiz. Av. Universidad de Cadiz 10, E-11519 Puerto Real-Cadiz, Spain; raul.ruizgarcia@uca.es (R.R.G); juanmanuel.vazquez@uca.es (J.M.V.M); jorge.salguero@uca.es (J.S.G).

* Correspondence: pedro.mayuet@uca.es; Tel.: +34-616-852-858

Abstract: The incorporation of plastic matrix composite materials into structural elements of the aeronautical industry requires contour machining and drilling processes along with metallic materials prior to final assembly operations. These operations are usually performed using conventional techniques, but they present problems derived from the nature of each material that avoid implementing One Shot Drilling strategies that work separately. In this work, the study focuses on the evaluation of the feasibility of Abrasive Waterjet Machining (AWJM) as a substitute for conventional drilling for stacks formed of Carbon Fiber Reinforced Plastic (CFRP) and aluminum alloy UNS A97050 through the study of the influence of abrasive mass flow rate, traverse feed rate and water pressure in straight cuts and drills. For the evaluation of the straight cuts, Stereoscopic Optical Microscopy (SOM) and Scanning Electron Microscopy (SEM) techniques are used inspection techniques have been used. In addition, the kerf taper through the proposal of a new method and the surface quality in different cutting regions have been evaluated. For the study of holes, the macrogeometric deviations of roundness, cylindricity and straightness have been evaluated. Thus, this experimental procedure reveals the conditions that minimize deviations, defects, and damage in straight cuts and holes obtained by AWJM.

Keywords: AWJM; Stack; CFRP; Aluminium UNS A97050; SOM/SEM; Kerf Taper; Surface Quality; Macrogeometric deviations.

---

1. Introduction

Over the last few decades, the aeronautical industry has been highlighted for its capacity to develop and manufacture structural elements built with advanced materials, having achieved a leading position in this area of activity with respect to other sectors.

In this sense, aeronautical industry has demonstrated its capacity for the development and manufacture of complex elements built with advanced materials. Thus, the main manufacturers (Airbus and Boeing) have increased the use of new materials, mainly plastic matrix composites, in combination with those traditionally used such as Duralumin alloys of 2XXX or the Al-Zn of 7XXX series with the aim of reducing aircraft weight, maintaining the structural integrity of the assembly. These materials have undoubted advantages linked to the demand of greater safety, and lower energy consumption and maintenance costs that characterize the air-transport today. Also, they provide an excellent relationship between mechanical strength and weight, rigidity and an increase in the life-cycle thanks to its good behaviour to fatigue and corrosion [1,2].

Most of the structural elements used in aircraft construction need to undergo different machining operations, mainly drilling or milling of contours, prior to assembly work through rivets in the Final Assembly Lines (FAL) [3,4]. During the assembly tasks in aeronautical structures, these materials are joined in form of stacks, which must be processed with drilling cycles under strict dimensional and geometric requirements, making difficult to keep these tolerances under control when the nature of the materials is different [5–8].

Indeed, the combination of materials of a different nature has a negative impact during machining operations. On the one hand, both the heterogeneity of the material and the abrasive behaviour of the carbon fibre negatively affect the tool life. Therefore, machining conditions and tool geometry must be adapted to these materials in order to reduce tool wear and thermal and mechanical defects produced during the cutting process, such as delamination or thermal damage to the composite matrix [9,10]. On the other hand, aluminium alloys tend to modify the geometry of the tool [11], especially by the development of adhesive phenomena such as Build Up Layer (BUL) or Build Up Edge (BUE) [5,12]. The union of these phenomena causes accelerated wear of the tool through the loss of geometry and the increase in temperature reached during the cutting process, which causes a reduction in tool life due to the synergy of the wear mechanisms produced.

This is compounded by problems at the stack interface, such as burring and cleaning due to accumulated chip residues. As a result, the drilling process is complex to carry out in a single step [13]. Instead, different successive drilling steps must be carried out until the final diameter is obtained, including cleaning the rework at the interface, which does not allow One Way Assembly (OWA) to be achieved as a key technology for process automation.

Alternatively, some authors have conducted studies of machining stacks with unconventional technologies such as laser or Abrasive Water Jet Machining (AWJM) [10,14–17]. In particular, AWJM has been widely studied as one of these machining alternatives, especially to replace contour milling processes [2,18]. This is mainly due to different factors that positively affect the surface integrity of the final parts. Among them, and in comparison with conventional machining processes, the absence of tool wear, the reduction of residual stresses induced on the surface of the material and the reduction of surface thermal damage as a result of low cutting temperatures should be highlighted [10,19,20].

However, the AWJM process shows its own limitations that lead to the appearance of specific defects during the cutting process, Figure 1. The most common defects in the process are the kerf taper, the Erosion Affected Zone (EAZ) and the formation of three possible different roughness zones along the machined surface [21]:

- Initial Damage Region (IDR). Area where the water jet hits on the material producing EAZ. The roughness in this region is high due to the abrasive particles impacting the material.
- Smooth Cutting Region (SCR). Region of variable thickness depending on the cutting parameters. It is the region with the best surface quality because it does not suffer the impact of particles and the jet still has enough kinetic energy to cut.
- Rough Cutting Region (RCR). Final region where the jet ends of cut material. The jet has lost enough cutting capacity and produces macro geometrical defects as striation marks.

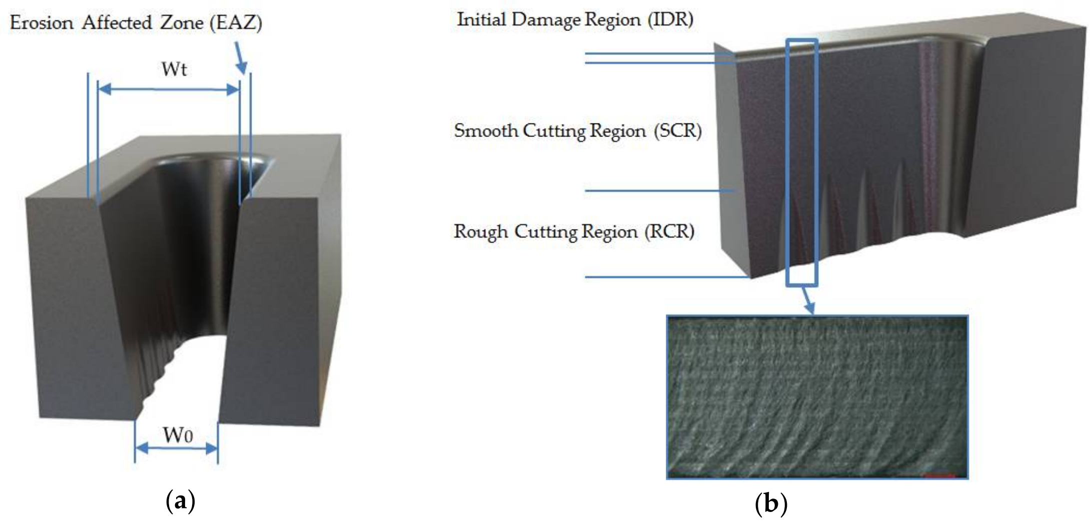

Peer-reviewed version available at Materials 2018, 12, 107; doi:10.3390/ma12010107

Figure 1. Scheme with the main defects associated with AWJM: (**a**) Erosion affected zone and kerf taper defined by inlet width (Wt) and outlet width (Wb); (**b**) Different roughness zones that can be formed in AWJM.

Specifically, the removal of material through AWJM is produced by erosion caused by particles that impact the material at high velocity and affect each material differently. In the case of carbon fibre reinforced with plastic matrix, the formation of the erosion process produces the breakage of the fibres and the degradation of the matrix. This prevents the layers of the material from remaining bonded causing the formation of initial cracks that result in delaminations when abrasive particles penetrate between the layers of the composite [22].

However, some characteristic defects in the final part may occur as a result of the effect of the combination of different parameters. In this article it is proposed to carry out a study based on the influence of the main cutting parameters on AWJM in order to reduce the appearance of the defects mentioned in stacks formed by the aluminium alloy UNSA97050 and CFRP. To this end, two experiments have been carried out based on the operations most required in the machining of aeronautical structures: straight cuts to analyse the cutting profile and drills to study the viability of the process. Finally, the state of the cuts has been evaluated through the use of microscopic inspection techniques and macro and microgeometric deviations.

2. Materials and Methods

For the experimental development, a plate of composite material CFRP AIMS 05-01-002 and another one of aluminium alloy UNS A97075 have been used. Both 5 mm thickness plates have been mechanically joined by 8 bolts to obtain two stack configurations: CFRP/UNS A97075 and UNS A97075/CFRP.

As technological parameters, combinations have been made for each configuration of the three most significant parameters: final water pressure (WP), abrasive mass flow (AMFR) and transverse feed capacity (TFR), due to the influence analyzed in [23]. The separation distance has been kept constant at 3 mm throughout the experimental phase and the abrasive selected is garnet with an average particle size of 80 µm in order to optimize aluminium penetration [24]. Under these considerations, the experimental design based on levels shown in Table 1 has been established.

To carry out the tests, two experimental blocks for each stack have been made. On the one hand, straight cuts were made in order to study the influence on the kerf taper and the different roughness zones. On the other hand, holes with a 8 mm diameter have been drilled to study macrogeometry. For this purpose, the experimental design and presimulation have been carried out using the CAD/CAM software Lantek® edition 34.02.02.02.02.02.02, making a total of 48 tests mechanized with a TCI water jet cutting machine model BPC 3020.

Table 1. Parameters used for each configuration

Test	WP (bar)	TFR (mm/min)	AMFR (g/min)
1	2500	15	170
2	2500	15	340
3	2500	30	170
4	2500	30	340
5	2500	45	170
6	2500	45	340
7	1200	15	170
8	1200	15	340
9	1200	30	170

 doi:10.20944/preprints201812.0007.v1

Peer-reviewed version available at *Materials* **2018**, *12*, 107; doi:10.3390/ma12010107

10	1200	30	340
11	1200	45	170
12	1200	45	340

For the evaluation of straight cuts, an optical evaluation of the machined material using Stereoscopic Optical Microscopy (SOM) and Scanning Electron Microscopy (SEM) techniques have been employed. A Nikon SMZ 800 stereo optical microscope was used for the SOM inspection and the Hitachi SU 1510 microscope was used for the SEM inspection. These techniques have been used to study the incrustation of abrasive particles in the IDR zone and in the delaminations produced. In addition, it has been used to generate a deeper measurement of the kerf taper. The literature tends to evaluate the taper as the difference between the cutting width of the water inlet and the cutting width of the water outlet depending on the thickness of the plate [17,19,25]. However, since the IDR may interfere with that extent, this paper proposes a new methodology based on image processing methods, for which ImageJ and Microsoft Excel® software have been used. It can be observed that this process concurs in a high variability depending on two measures (W_t and W_b). Therefore, in this work a new procedure is proposed that consists of capturing the image of the cut and its subsequent digitalization in ten points with a non-linear distribution, as shown in Figure 2.

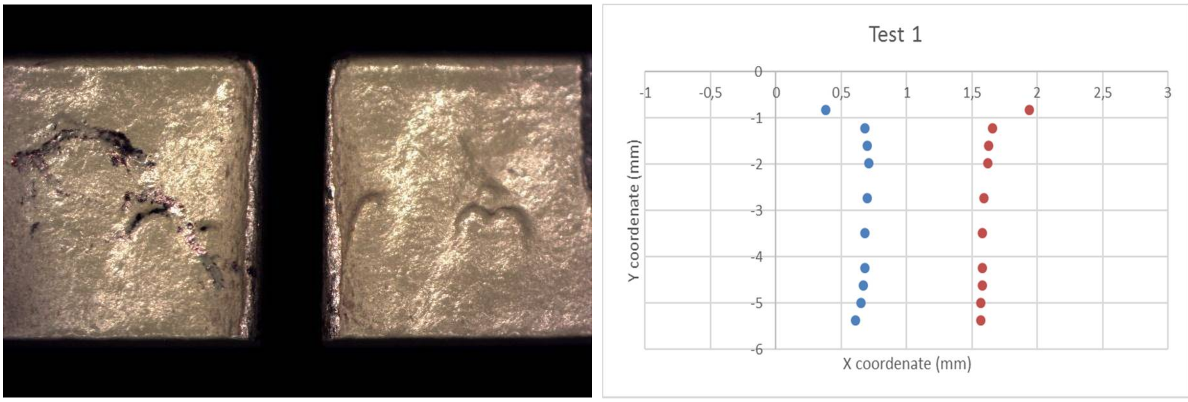

(a) (b)

Figure 2. Proposal of measurement of the kerf taper from: (a) SOM image and (b) geometry discretization.

For the measurement of roughness, the Mahr Perthometer Concept PGK 120 (Mahr, Göttingen, Germany) has been employed to analyse the Ra of the specimens in each test in different zones coinciding with IDR, SCR and RCR, Figure 3.

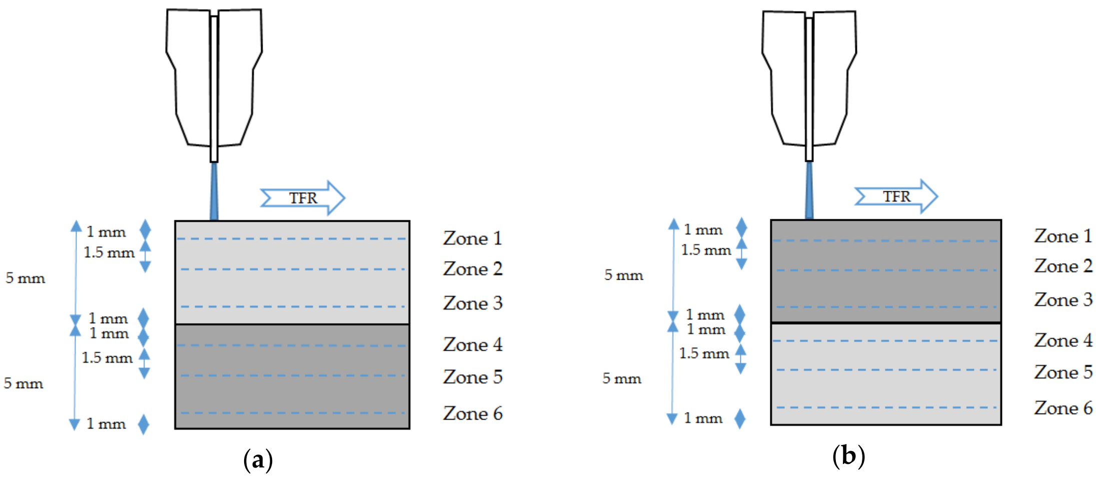

 doi:10.20944/preprints201812.0007.v1

Peer-reviewed version available at *Materials* **2018**, *12*, 107; doi:10.3390/ma12010107

Figure 3. Schematic representing the roughness measurement zones and the distance between them for: (a) UNS A97075/CFRP configuration; (b) CFRP/UNS A97075 configuration.

For the evaluation of the holes, a station of measurement Mahr MMQ44 Form Tester (Mahr, Göttingen, Germany) has been used to measure the roundness at the entrance and exit of the drill in each material, the cylindricity of the entire profile of the drill, and the straightness in four separate generatrices to 90°. To analyze the macrogeometric deviations, replicas of the holes due to the impossibility of direct measuring on the material have been fabricated. These replicas have been made with a polymer type F80 Ra (R.G.X, Plastiform, Madrid, Spain) with the ability to guarantee stability during the measurement process for diameters greater than 4 mm.

Finally, to distinguish the most significant parameters for evaluation results, analysis of variance (ANOVA) for a 95% confidence interval has been employed. After that, contour charts for each variable studied in the experimental have been obtained.

3. Results and Discussion

3.1. Straight Cuts Evaluation

3.1.1. SOM/SEM Evaluation

In order to detect possible defects in the tests, SOM inspection was carried out parallel and perpendicular to the direction of TRF. First, to ease later kerf study, images were taken from the machine feed direction from both united stack and independent parts as shown in Figure 4. The images show the influence of the opening of the jet at the entrance of the material producing an increase in the width of kerf. This phenomenon is related to damages produced in the IDR zone [23].

(a) (b) (c)

Figure 4. SOM image of the cutting front in: (a) Stack CFRP/UNS A97075; (b) CFRP plate; (c) UNS A97075 plate

On the other hand, Figure 5 shows the profile of CFRP specimens in order to identify delaminations. In order to visualize the delamination along the machined surface, several images were taken showing the absence of visible delamination after machining in the test performed with the parameters considered to be the most aggressive.

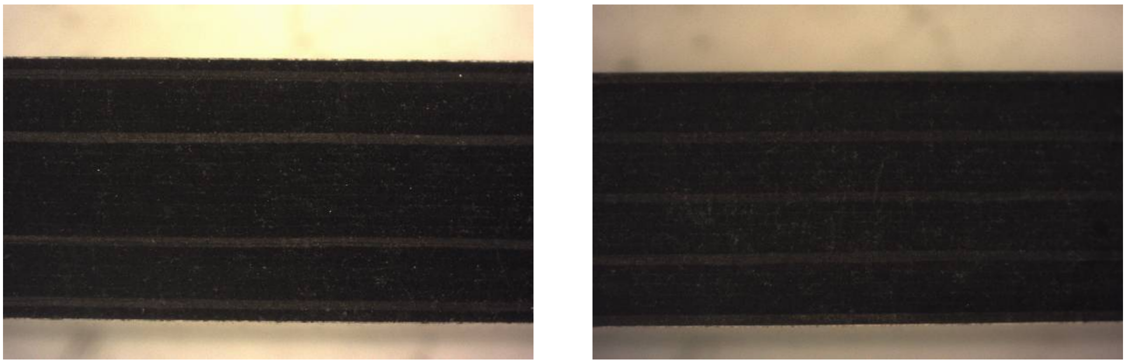

(a) (b)

Figure 5. SOM image of CFRP profile. Test 2. WP = 2500 bar, TFR = 15 mm/min and AMFR = 340 gr/min for: (a) UNS A97075/CFRP; (b) CFRP/UNS A97075.

In order to obtain a more detailed microscopic analysis of the samples, images have been taken using SEM microscopy. Thus, Figure 6 shows the results of the SEM inspection in CFRP showing that no delamination was detected. However, Figure 4 (c) shows in detail the state of the specimen entrance zone where signs of impact deformation and particle drag have been observed. This state extends to the interface reflecting that a percentage of particles have lodged in the space between the two materials.

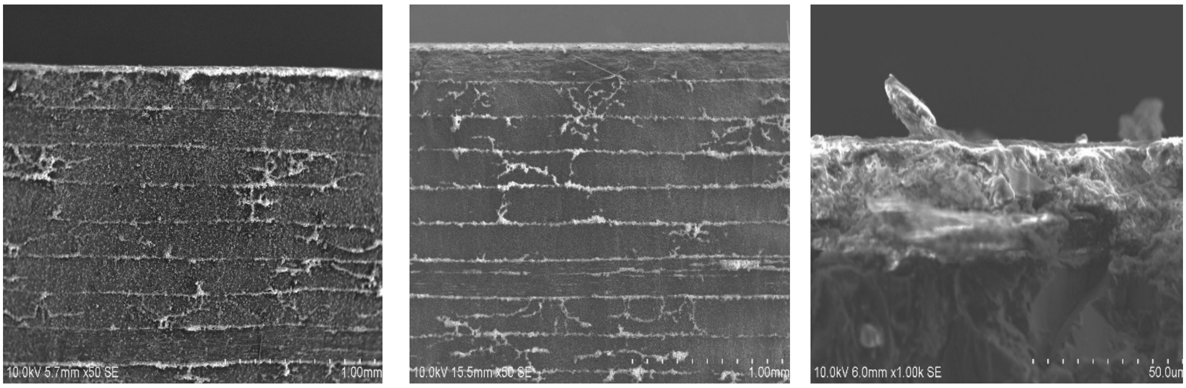

(a) (b) (c)

Figure 6. SEM image of CFRP profile. Test 2. WP = 2500 bar, TFR = 15 mm/min and AMFR = 340 gr/min for (a)UNS A97075/CFRP; (b) CFRP/UNS A97075; (c) Interface over CFRP.

As for aluminium alloy, SOM study showed a series of dark coloured streaks along the profile that repeated for both configurations to a greater or lesser extent depending on the energy of the jet. Specifically, Figure 7 (a) shows the marks mentioned at the bottom while Figure 7 (b) at the top. This phenomenon together with the colour of the stretch mark seems to indicate that they are located in the zone close to the contact with the carbon fibre. Finally, Figure 7 (c) shows the result of the study for test 11 where no transfer of carbon fibre to aluminium is observed, possibly due to the lower energy and the quantity abrasive particles used.

Preprints (www.preprints.org) | NOT PEER-REVIEWED | Posted: 3 December 2018 doi:10.20944/preprints201812.0007.v1

Peer-reviewed version available at Materials 2018, 12, 107; doi:10.3390/ma12010107

(a) (b) (c)

188 **Figure 7.** Profile SOM of UNS A97075 from: (a) UNS A97075/CFRP. Test 2. WP = 2500 bar, TFR = 15
189 mm/min and AMFR = 340 gr/min; (b) CFRP/UNS A97075. Test 2. WP = 2500 bar, TFR = 15 mm/min
190 and AMFR = 340 gr/min;(c) CFRP/UNS A97075. Test 11. WP = 1200 bar, TFR = 45 mm/min and AMFR
191 = 170 gr/min.

192 In an attempt to obtain more information on the marks observed in Figure 7, the SEM/EDS
193 inspection of aluminium has focused on discovering the state of the aluminium and the nature of
194 these marks. Initially, Figures 8 (a) and (b) show the state of the material at the inlet. In a detailed
195 way, the embedded particles and the deformation produced during the cutting process are
196 appreciated, coinciding with the IDR or zone 1.
197

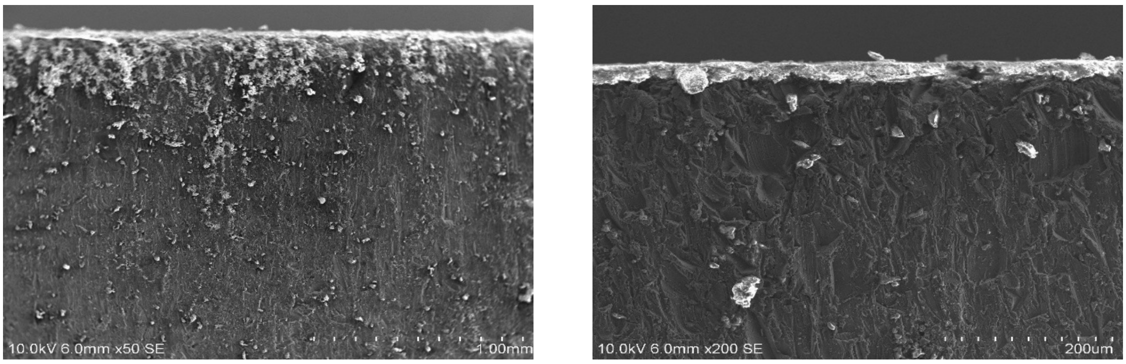

(a) (b)

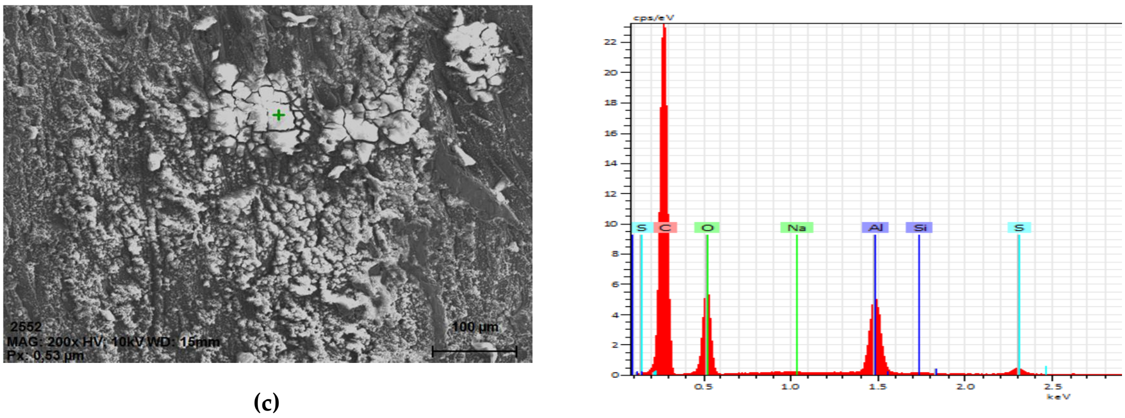

(c)

(d)

198 **Figure 8.** Test 2 SEM evaluation: (a) Abrasive imbued into UNS A97075; (b) Abrasive particles in the
199 interface and channel created over the material; (c) Remains of carbon and point of EDS; (d) EDS results
200 with a peak on the carbon.

Preprints (www.preprints.org) | NOT PEER-REVIEWED | Posted: 3 December 2018 doi:10.20944/preprints201812.0007.v1

Peer-reviewed version available at *Materials* **2018**, *12*, 107; doi:10.3390/ma12010107

On the other hand, figures 8 (c) and (d) show the stain examined in the striations observed by SOM microscopy and the results of the EDS analysis, respectively. The EDS analysis revealed the high presence of carbon at this point, confirming the carry-over of carbon particles during machining from one material to another. It should be noted that no traces of aluminium deposited on the carbon fibre have been detected.

To analyse the state of the aluminium outside the zone of the stretch marks, another EDS spot was carried out outside those stains and showed almost no carbon and a huge peak on aluminium. As a direct conclusion it appears that particles from composite are swept for the water beam and because of the water high energy, they end up embedded into UNS A97075. It seems like composite deposition over aluminium has a direct correlation with beam penetration capacity.

So, contrary to what one would expect, a higher abrasive pressure and flow has not resulted in an increase in delaminations for both configurations. Similarly, the inclusion of abrasive particles has not greatly increased within the parameters studied. However, an increase in the inclusion of carbon particles in the aluminium alloy has been observed as the pressure increases.

3.1.2. Kerf Taper evaluation

The ANOVA analysis performed showed that AMFR and TFR parameters have been the most influential in taper formation. Average kerf taper values for each material when the configuration UNS A97075/CFRP is set are shown in Figure 9. The same values for configuration CFRP/UNS A97075 are shown in Figure 10.

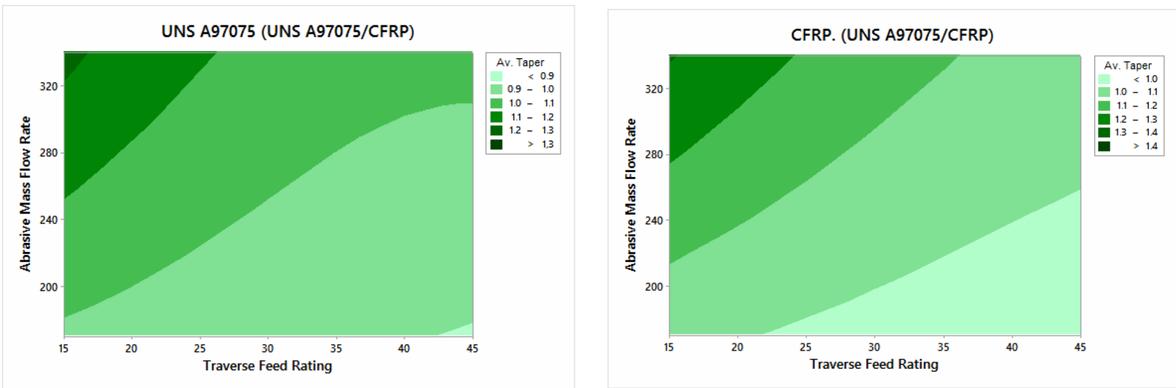

(a) **(b)**

Figure 9. Average kerf taper for USN A97075/CFRP configuration: (a) UNS A97075; (b) CFRP.

Taking into account that the diameter of the jet is 0.74 mm, the data that approximate this value are those that will have the lowest values of taper according to the average established between all the measurements.

In this way, the data represented in figures 9 and 10 show that the taper is reduced as AMFR decreases and TFR increases, showing the best results for TFR = 45 mm/min and AMFR = 170 gr/min, in accordance with [25].

This behaviour is shared with the CFRP behaviour in CFRP/UNS A97075 configuration. Figure 10 b, however, shows a very different behaviour. This change is due to the lesser energy of the water beam when it collides with the aluminium. Since a percentage of energy is transformed during the CFRP machining, it appears that the AMFR is the determinant parameter when the cut's wide is examined. As for the differences between the two material configurations, figure 10 shows that when the jet directly affects the carbon fibre, the taper generated for the best parameter ratio reaches values higher than 1.2 compared to the value 1 reached for the UNS A97075/CFRP configuration. This shows the difference in the mechanical properties of each material, offering greater resistance to penetration the metallic material.

Preprints (www.preprints.org) | NOT PEER-REVIEWED | Posted: 3 December 2018 doi:10.20944/preprints201812.0007.v1

Peer-reviewed version available at Materials 2018, 12, 107; doi:10.3390/ma12010107

Overall, a similar behaviour is observed between the materials located in the upper and lower part of the stack. Despite this, a smaller taper is always observed in UNS A97075 than in CFRP.

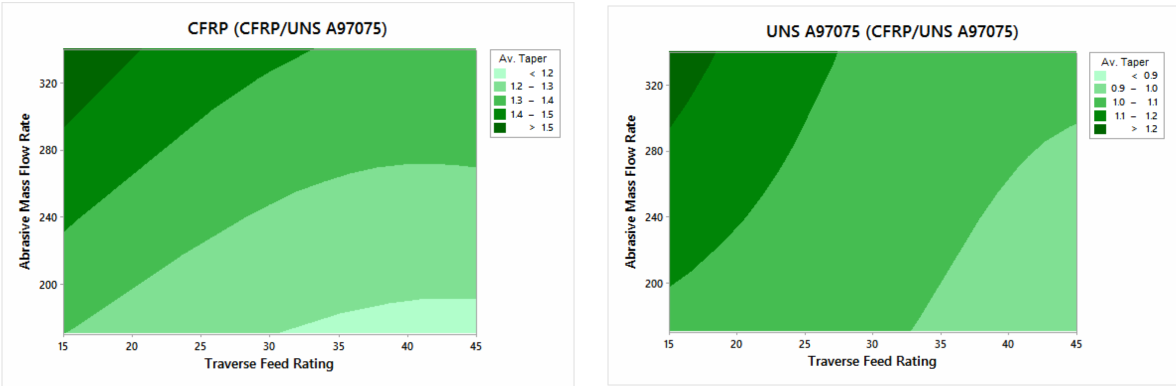

(a) (b)

Figure 10. Average kerf taper for CFRP/USN A97075/ configuration: (a) CFRP; (b) UNS A97075.

3.1.3. Surface roughness

The influential parameters in the analysis of surface quality are also AMFR and TFR for both configurations. In this case, given the importance of roughness zones, all evaluated data are shown in Appendix A.

Figure 11 shows the results of the UNS A97075/CFRP configuration. A tendency to increase the average roughness can be observed as TFR increases and AMFR decreases. Figure 12, on the other hand, shows the results of CFRP/UNS A97075 configuration. The same trend as in Figure 11 is observed although there is a greater difference between the material placed at the top and bottom.

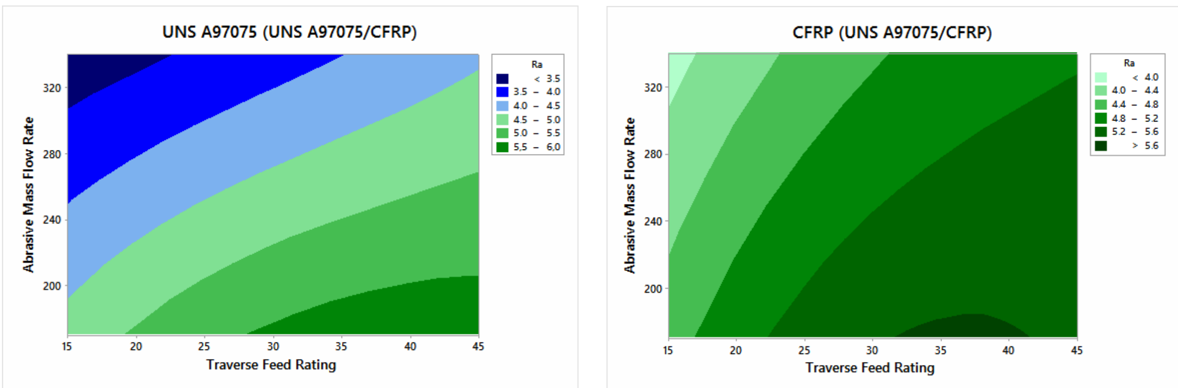

(a) (b)

Figure 11. Average roughness for UNS A97075/CFRP configuration: (a) UNS A97075 and (b) CFRP.

Despite of the fact that increasing AMFR has to increase the number of particles collisions during the machining, it seems that it also ensures a lesser value of average roughness for UNS A97075/CFRP configuration. In fact, its effect seems to be especially determinant over the material placed on the bottom of the stack as could be seen in Figure 11(b).

However, the configuration CFRP/UNS A97075 shows the opposite tendency. It seems like TFR is much more an influencing parameter than the AMFR regarding the minimization of average roughness.

Both of these behaviors could be explained regarding kerf taper results. It seems that in order to achieve a minor average roughness in the material placed at the bottom, the most important

Preprints (www.preprints.org) | NOT PEER-REVIEWED | Posted: 3 December 2018 doi:10.20944/preprints201812.0007.v1

Peer-reviewed version available at Materials 2018, 12, 107; doi:10.3390/ma12010107

parameter is the wide of the cut on the material placed on the top of the stack. This reduces particles collisions and reduces water beam energy loss.

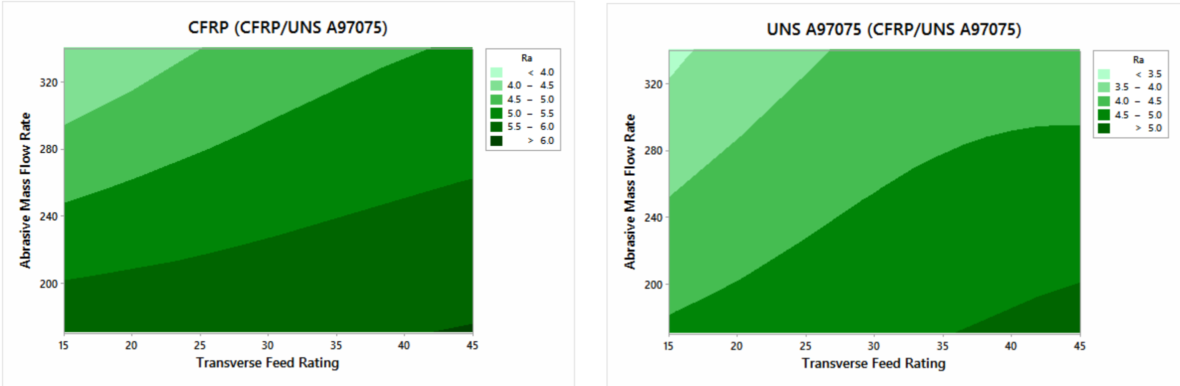

(a) (b)

Figure 12. Average roughness for CFRP/USN A97075 configuration: (a) CFRP and (b) UNS A97075.

It is observed that the maximum roughness of the material placed at the bottom of the stack, regardless of its nature, has lower values. In addition, the maximum roughness never exceeds 7 μm in any test. A more in-depth analysis of the data based on Appendix A reflects this. On the one hand, the area with the greatest damage is region 1 or IDR due to deformations and damage caused by the impact of the jet on the material. In addition, this is the region where embedded particles have been detected. On the other hand, the material at the bottom has lower roughness values in region 4 due to the protection of the material at the top.

On the other hand, it can be observed that regions 2 and 5, corresponding to SCR, do not have values lower than those recorded in zones 3 and 6 as RCR. This indicates the existence of two zones because the jet still has enough kinetic energy to make the cut without the appearance of striations.

3.2. Holes Evaluation

3.2.1. Roundness deviation

Figure 13 shows the data obtained from roundness deviations for each material and the total average of both materials. In this way, the results can be analyzed separately.

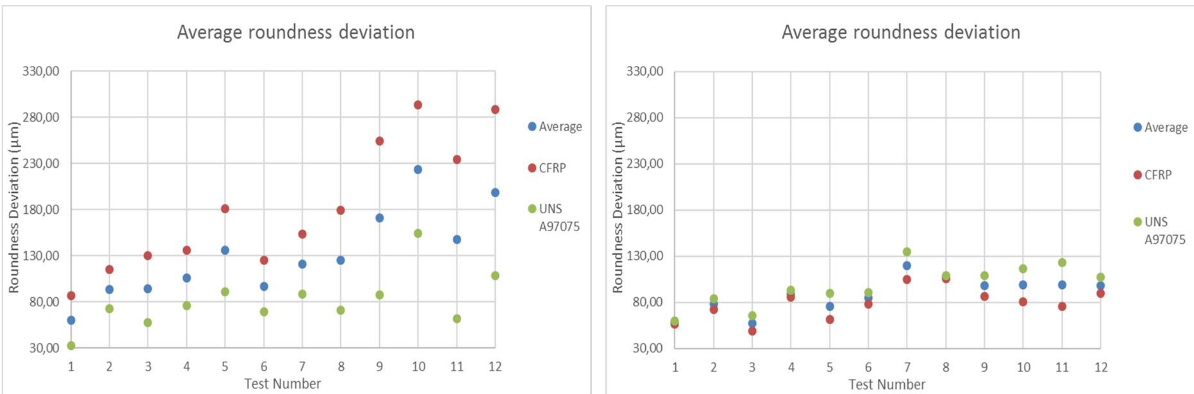

(a) (b)

Figure 13. Average roundness: (a) UNS A97075/CFRP configuration; (b) CFRP/UNS A97075 configuration.

Figure 13 (a) shows the data for UNS A97075/CFRP configuration. The data show that in all tests the deviation is higher for CFRP even though it is the material located at the bottom of the stack. This

Preprints (www.preprints.org) | NOT PEER-REVIEWED | Posted: 3 December 2018 doi:10.20944/preprints201812.0007.v1

Peer-reviewed version available at *Materials* **2018**, *12*, 107; doi:10.3390/ma12010107

is due to the fact that the erosion and removal of composite materials is different from that produced in metallic materials. Thus, in CFRP the particles weaken and remove the matrix of the compound to subsequently break the fibres of the adjacent zone [2]. This phenomenon, combined with the material's resistance to jet dispersion as a result of the loss of energy after cutting the aluminium, leads to an increase in the deflection in this material. This deflection increases considerably as WP decreases and TFR increases, which makes sense because these are tests with lower shear power.

On the other hand, Figure 13 (b) shows the results of CFRP/UNS configuration A97075. In this particular case, the deviations follow a similar relationship to that of the previous case in terms of parameter influence, although it is true that the difference in the measured values is high. Thus, although in this case the aluminium is at the bottom of the pile, it seems that the expansion of the water jet does not deform the entry zone due to the differences in terms of removal of material explained in the previous paragraph. This results in homogeneous deviations in roundness between the two configurations, which favours a subsequent joint by means of rivets.

3.2.2. Cylindricity deviation

Cylindricity deviation has also been measured with two measures for each material and configuration. However, due to the nature of the test, only one value result as output. Appendix D contains all collected data. Nevertheless, an ANOVA description of variables influence is shown in Figure 14.

The ANOVA analysis carried out shows that the parameters that have the greatest influence on the formation of the deviations are WP and TFR. Specifically, Figure 14 shows that the UNS configuration A97075/CFRP has lower cylindricity deviation values, which is in good agreement with the taper values obtained. This is due to the close relationship between both parameters. In order to offer a better correlation of results, the profiles measured for test 11 are presented as an example, Figure 15.

A more detailed description of the data reflects that cylindricity decreases as TFR decreases and WP increases. Specifically, Figure 14 (a) reveals that TFR has a superior influence when the alloy is at the inlet of the material which reflects the importance of employing reduced feed rates to prevent its formation. As for figure 15, both (a) and (b) shows CFRP on the bottom and UNS A97075 on the top of the cone. It can be observed how it affects the energy loss to the generated hole, especially in Figure 15 (a).

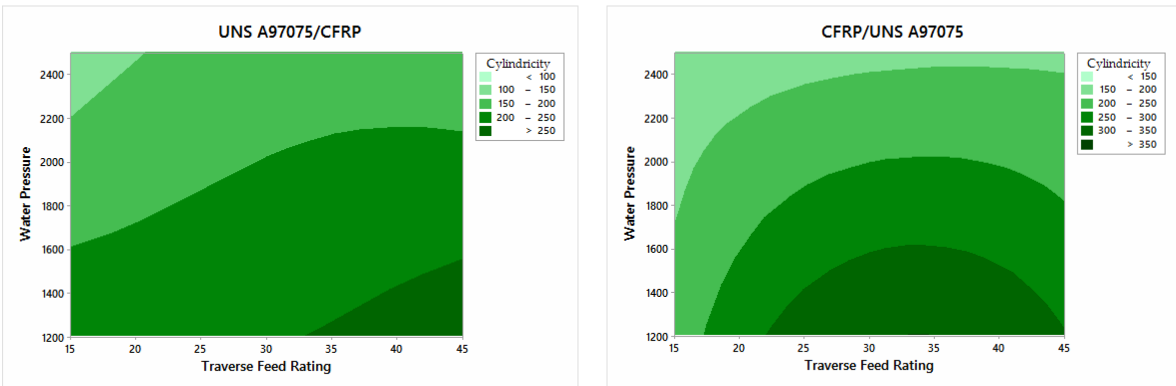

(a) **(b)**

Figure 14. Cylindricity results on: (a) UNS A97075/CFRP configuration; (b) CFRP/UNS A97075 configuration.

Preprints (www.preprints.org) | NOT PEER-REVIEWED | Posted: 3 December 2018 doi:10.20944/preprints201812.0007.v1

Peer-reviewed version available at *Materials* **2018**, *12*, 107; doi:10.3390/ma12010107

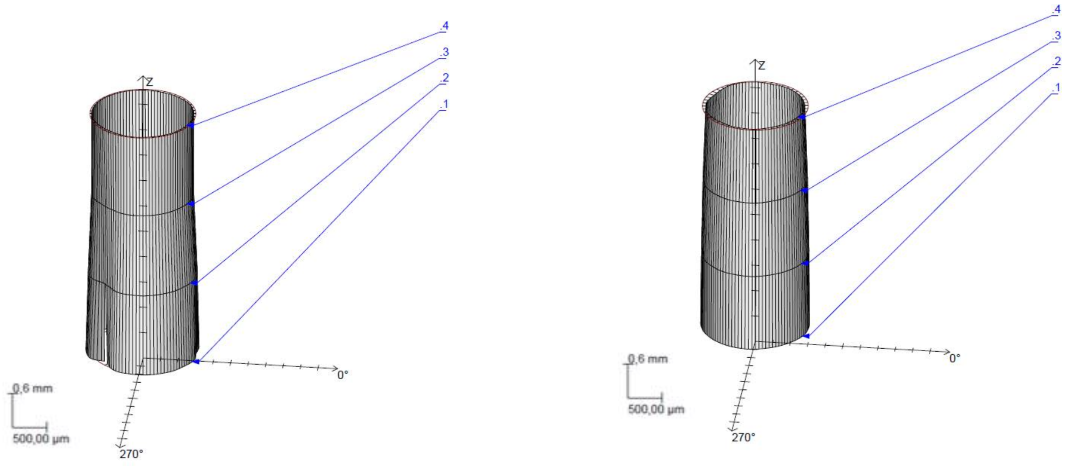

(a) **(b)**

Figure 15. Cylindricity deviations. Test 11. WP = 1200 bar, TFR = 45 mm/min and AMFR = 170 gr/min for: (a) UNS A97075/CFRP configuration; (b) CFRP/UNS A97075 configuration.

3.2.3. Straightness deviation

In this case, there is no distinction between materials and straightness has been evaluated throughout the entire profile. Thus, Figure 15 shows a comparison between the values obtained for the two configurations.

As a general conclusion, a higher water jet drilling capacity means less straightness deviation. It is also observed that the CFRP/UNS A97075 configuration shows better results for the same test number except for the last three tests which, due to their lower drilling capacity due to the use of lower WP and TFR, are not able to maintain a uniform cutting profile of the aluminium alloy and therefore cannot maintain straightness along the hole.

The results reveal that the data in configuration UNS A97075/CFRP are slightly lower than those recorded in configuration CFRP/UNS A97075. In addition, it should be noted that for high pressures the straightness deviation increases when the compound is located at the top.

On the other hand, it should be noted that the standard deviation presented by the results is high, which makes it difficult to establish relationships between the results.

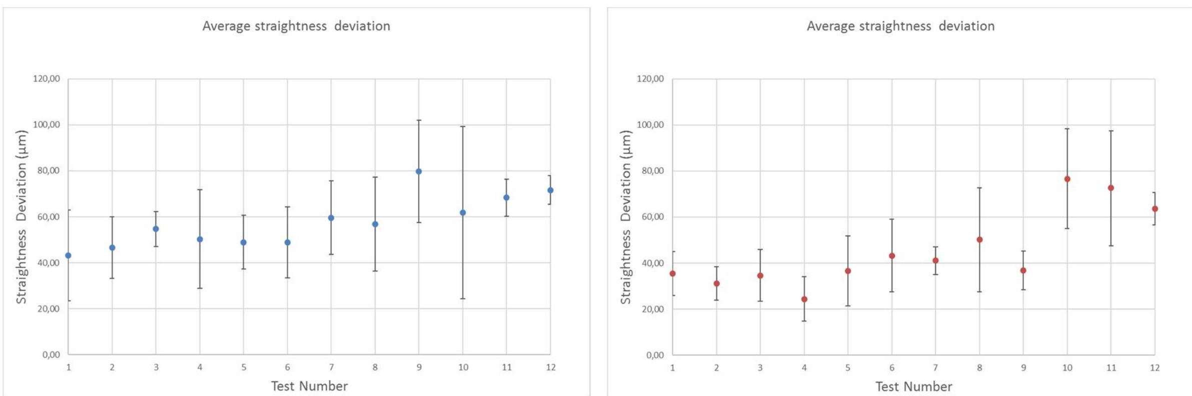

(a) **(b)**

Figure 15. Straightness deviations results on: (a) UNS A97075/CFRP configuration; (b) CFRP/UNS A97075 configuration

4. Conclusions

A study has been carried out on the influence of the parameters of the abrasive water jet on the quality of straight cuts and holes in composite materials and aeronautical aluminium. Based on this, the following conclusion can be drawn:

1. The machining of straight cuts has revealed that thermal damage is eliminated and the appearance of delamination in CFRP is reduced. Thus, for the selected parameters, no delamination has been found in the mechanized test samples.
2. The proposed kerf taper measurement method has been validated for measurement in stacks. The results show the influence of the selected parameters obtaining the best results for high TFR and AMFR for both configurations, especially USN A97075/CFRP, with CFRP being the material with the highest kerf taper. On the other hand, the CFRP/UNS A97075 configuration has lower microgeometric deviations for the three evaluated parameters due to the lower loss of jet energy.
3. Ra is in all cases below 7 µm, although this value is specific for tests 9, 10, 11 and 12. The functional holes show a lower roughness for both materials in any configuration. Nevertheless, it appears that the UNS A97075/CFRP configuration offers a better roughness of the holes.
4. The study of surface quality has revealed that the IDR zone of the second material (region 4) is attenuated from impacts of particle and EAZ impacts. On the other hand, the presence of RCR has not been detected.
5. The measurements obtained of roundness present a greater deviation at the entrance of the drill due to the IDR zone in region 1, independently of the selected configuration, although it is true that the CFRP/UNS A97050 configuration presents values around 200% lower for the tests with lower penetration power (9, 10, 11 and 12).
6. The influence of kerf taper on cylindricity deviations has been reflected through the evaluated profiles, recording that the parameters with the greatest influence on its formation are WP and TFR. In this case the configuration UNS A97075/CFRP presents better results of cylindricity.
7. The straightness deviations have not allowed to establish consolidated conclusions due to the high standard deviation registered. However, it can be seen once again that tests 9, 10, 11 and 12 have higher values.

Finally, it should be noted that this process does not generate burrs in metallic materials due to its abrasive nature or thermal gradients that damage the material. On the other hand, it should be noted that each configuration has different characteristics, but it is the UNS A97075/CFRP configuration that presents the best results in terms of macro and microgeometric deviations.

Author Contributions: Conceptualization, R.R.G and P.F.M.A.; Methodology, R.R.G and P.F.M.A.; Software, R.R.G and J.S.G; Validation, P.F.M.A. and J.M.V.M.; Formal Analysis, P.F.M.A. and J.M.V.M.; Investigation, R.R.G and P.F.M.A.; Resources, J.M.V.M. and J.S.G.; Data Curation, R.R.G and J.M.V.M.; Writing-Original Draft Preparation, R.R.G.; Writing-Review & Editing, P.F.M.A. and J.S.G.; Visualization, P.F.M.A. and J.M.V.M.; Supervision, P.F.M.A; Project Administration, J. S.G.; Funding Acquisition, J.S.G.

Funding: This work has received financial support from Special Actions for the Transfer of the Programme for the Promotion and Promotion of the Research and Transfer Activity of the University of Cadiz.

Conflicts of Interest: The authors declare no conflict of interest.

Appendix A

Table A 1. Average roughness UNS A97075/CFRP configuration

UNS A97075/CFRP Configuration Ra (μm)													
	Test	1	2	3	4	5	6	7	8	9	10	11	12
Al (inlet)	region 1	4,95	4,00	6,73	4,74	6,68	6,43	7,39	3,36	8,00	3,76	8,22	5,05
	region 2	3,52	2,78	4,34	4,01	4,66	3,84	4,19	2,88	5,05	3,23	5,45	3,82
	region 3	4,22	3,45	4,79	3,27	5,04	3,79	3,87	2,85	4,58	3,69	4,70	3,64
CFRP (Outlet)	region 4	4,99	3,72	5,77	4,42	5,48	4,73	4,36	3,30	5,44	4,24	4,49	4,72
	region 5	5,39	4,48	5,54	4,42	6,31	4,94	4,31	3,84	5,89	5,07	5,98	5,40
	region 6	4,19	3,99	5,27	4,43	4,20	4,27	4,49	3,77	5,45	5,90	6,53	7,00

Table A 2. Average roughness CFRP /UNS A97075 configuration

CFRP/ UNS A97075 Configuration Ra (μm)													
	Test	1	2	3	4	5	6	7	8	9	10	11	12
CFRP (inlet)	region 1	6,99	4,79	7,80	5,66	7,46	6,52	8,36	4,01	7,89	5,08	7,59	5,97
	region 2	4,78	3,80	5,04	4,49	5,38	4,34	5,00	3,54	5,17	4,54	5,00	4,40
	region 3	4,96	3,91	4,97	4,25	5,13	4,78	4,97	3,94	4,56	4,10	5,64	4,27
Al (Outlet)	region 4	4,54	3,42	5,12	4,17	5,19	4,01	4,57	3,55	4,62	4,19	4,48	4,06
	region 5	4,68	3,21	4,82	3,81	5,21	4,08	4,27	3,35	4,88	4,58	5,69	4,73
	region 6	4,22	3,12	5,11	3,35	5,31	4,24	5,20	3,63	4,79	4,54	5,10	4,44

References

1. Bazli, M.; Ashrafi, H.; Jafari, A.; Zhao, X.L.; Gholipour, H.; Oskouei, A.V. Effect of thickness and reinforcement configuration on flexural and impact behaviour of GFRP laminates after exposure to elevated temperatures, *Compos. Part B Eng.* **2019**, *157*, 76–99, doi:10.1016/j.compositesb.2018.08.054.
2. Hejjaji, A.; Zitoune, R.; Crouzeix, L.; Le Roux, S.; Collombet, F. Surface and machining induced damage characterization of abrasive water jet milled carbon/epoxy composite specimens and their impact on tensile behavior, *Wear*, **2017**, *376–377*, 1356–1364, doi:10.1016/j.wear.2017.02.024.
3. Casalegno, V.; Salvo, M.; Rizzo, S.; Goglio, L.; Damiano, O.; Ferraris, M. Joining of carbon fibre reinforced polymer to Al-Si alloy for space applications, *Int. J. Adhes. Adhes* **2018**, *82*, 146–152, doi:10.1016/j.ijadhadh.2018.01.009.

4. Lambiase, F.; Durante, M.; Di Ilio, A. Fast joining of aluminum sheets with Glass Fiber Reinforced Polymer (GFRP) by mechanical clinching, *J. Mater. Process. Technol* **2016** *236* 241–251, doi:10.1016/j.jmatprotec.2016.04.030.
5. Park, K.H.; Beal, A.; Kim, D.D.W.; Kwon, P.; Lantrip J. Tool wear in drilling of composite/titanium stacks using carbide and polycrystalline diamond tools, *Wear* **2011**, *271*, 2826–2835, doi:10.1016/j.wear.2011.05.038.
6. Ramulu, M.; Branson, T. ; Kim, D. A study on the drilling of composite and titanium stacks, *Compos. Struct.* **2001**, *54*, 67–77, doi:10.1016/S0263-8223(01)00071-X.
7. Zitoune, R.; Krishnaraj, V.; Collombet, F. Study of drilling of composite material and aluminium stack, *Compos. Struct.* **2010**, *92*, 1246–1255, doi:10.1016/j.compstruct.2009.10.010.
8. Kuo, C.; Li, Z.; Wang, C. Multi-objective optimisation in vibration-assisted drilling of CFRP/Al stacks, *Compos. Struct.* **2017**, *173*, 196-209, doi:10.1016/j.compstruct.2017.04.026.
9. Saleem, M.; Toubal, L.; Zitoune, R.; Bougherara, H. Investigating the effect of machining processes on the mechanical behavior of composite plates with circular holes, *Compos. Part A Appl. Sci. Manuf.* **2013**, *55*, 169–177, doi:10.1016/j.compositesa.2013.09.002.
10. Alberdi, A.; Artaza, T.; Suárez, A.; Rivero, A.; Girot, F. An experimental study on abrasive waterjet cutting of CFRP/Ti6Al4V stacks for drilling operations, *Int. J. Adv. Manuf. Technol*. **2016**, *86*, 691–704, doi:10.1007/s00170-015-8192-x.
11. D'Orazio, A.; El Mehtedi, M.; Forcellese, A.; Nardinocchi, A.; Simoncini, M. Tool wear and hole quality in drilling of CFRP/AA7075 stacks with DLC and nanocomposite TiAlN coated tools, *J. Manuf. Process*. **2017**, *30*, 582–592, doi:10.1016/j.jmapro.2017.10.019.
12. Zitoune, R.; Krishnaraj, V.; Sofiane Almabouacif, B.; Collombet, F.; Sima, M.; Jolin, A. Influence of machining parameters and new nano-coated tool on drilling performance of CFRP/Aluminium sandwich, *Compos. Part B Eng*. **2012** ,*43*, 1480–1488, doi:10.1016/j.compositesb.2011.08.054.
13. Wang, F.; Qian, B.; Jia, Z.; Fu, R.; Cheng, D. Secondary cutting edge wear of one-shot drill bit in drilling CFRP and its impact on hole quality, *Compos. Struct.* **2017**, *178*, 341–352, doi:10.1016/j.compstruct.2017.04.024.
14. El-Hofy, M.; Helmy, M.O.; Escobar-Palafox, G.; Kerrigan, K.; Scaife, R.; El-Hofy, H.; Abrasive Water Jet Machining of Multidirectional CFRP Laminates, *Procedia CIRP*. **2018**, *68*, 535–540, doi:10.1016/j.procir.2017.12.109.
15. Schwartzentruber, J.; Spelt, J.K.; Papini, M.; Prediction of surface roughness in abrasive waterjet trimming of fiber reinforced polymer composites, *Int. J. Mach. Tools Manuf.* **2017**, *122*, 1–17, doi:10.1016/j.ijmachtools.2017.05.007.
16. Yuvaraj, N.; Kumar, M.P. Cutting of aluminium alloy with abrasive water jet and cryogenic assisted abrasive water jet: A comparative study of the surface integrity approach, *Wear.* **2016**,*362–363*, 18–32, doi:10.1016/j.wear.2016.05.008.
17. MM, I.W.; Azmi, A.; Lee, C.; Mansor, A. Kerf taper and delamination damage minimization of FRP hybrid composites under abrasive water-jet machining, *Int. J. Adv. Manuf. Technol*. **2018**, *94*, 1727–1744, doi:10.1007/s00170-016-9669-y.
18. Ramalingam, T.; Bhaskar, S.; Seshumadhav, K.; Allamraju, K.V. Optimization of process parameters in bi-directional carbon fiber composite using AWJM, *Mater. Today Proc.* **2018**, *5*, 18933–18940, doi:10.1016/j.matpr.2018.06.243.
19. Alberdi, A.; Suárez, A.; Artaza, T.; Escobar-Palafox, G.A.; Ridgway, K. Composite Cutting with Abrasive Water Jet, *Procedia Eng*. **2013**, *63*, 421–429, doi:10.1016/j.proeng.2013.08.217.
20. Unde, P.D.; Gayakwad, M.D.; Patil, N.G.; Pawade, R.S.; Thakur, D.G.; Brahmankar, P.K.; Experimental Investigations into Abrasive Waterjet Machining of Carbon Fiber Reinforced Plastic, *J. Compos*. **2015**, *2015*, 1–9, doi:10.1155/2015/971596.
21. Ravi Kumar, K.; Sreebalaji, V.S.; Pridhar, T. Characterization and optimization of Abrasive Water Jet Machining parameters of aluminium/tungsten carbide composites, *Meas. J. Int. Meas. Confed*. **2018**, *117*, 57–66, doi:10.1016/j.measurement.2017.11.059.
22. Shanmugam, D.K.; Nguyen, T.; Wang, J. A study of delamination on graphite/epoxy composites in abrasive waterjet machining, Compos. *Part A Appl. Sci. Manuf.* **2008**, *39*, 923–929, doi:10.1016/j.compositesa.2008.04.001.

23. Mayuet, P.F.; Girot, F.; Lamíkiz, A.; Fernández-Vidal, S.R.; Salguero, J.; Marcos, M. SOM/SEM based Characterization of Internal Delaminations of CFRP Samples Machined by AWJM, *Procedia Eng*. **2015**, *132*, 693–700, doi:10.1016/j.proeng.2015.12.549.
24. Shukla, R.; Singh, D. Experimentation investigation of abrasive water jet machining parameters using Taguchi and Evolutionary optimization techniques, *Swarm Evol. Comput*. **2017**, *32*, 167–183, doi:10.1016/j.swevo.2016.07.002.
25. Gupta, V.; Pandey, P.M.; Garg, M.P.; Khanna, R.; Batra, N.K. Minimization of Kerf Taper Angle and Kerf Width Using Taguchi's Method in Abrasive Water Jet Machining of Marble, *Procedia Mater. Sci*. **2014**, *6*, 140–149, doi:10.1016/j.mspro.2014.07.017.